J. Appl. Comput. Mech., 5(5) (2019) 976-988
DOI: 10.22055/JACM.2019.27997.1449

ISSN: 2383-4536
jacm.scu.ac.ir

M&MoCS
Shahid Chamran University of Ahvaz

Journal of
Applied and Computational Mechanics

Research Paper

MHD Flow and Heat Transfer of SiC-TiO_2/DO Hybrid Nanofluid due to a Permeable Spinning Disk by a Novel Algorithm

Behnam Fallah[1], Saeed Dinarvand[1], Mohammad Eftekhari Yazdi[1], Mohammadreza Nademi Rostami[1], Ioan Pop[2]

[1] Department of Mechanical Engineering, Islamic Azad University, Central Tehran Branch, Tehran, Iran
[2] Department of Applied Mathematics, Babeş-Bolyai University, 400084 Cluj-Napoca, Romania

Received December 25 2018; Revised March 10 2019; Accepted for publication March 11 2019.
Corresponding author: S. Dinarvand, sae.dinarvand@iauctb.ac.ir; saeed_dinarvand@yahoo.com

Abstract. This study intends to semi-analytically investigate the steady 3D boundary layer flow of a SiC-TiO_2/DO hybrid nanofluid over a porous spinning disk subject to a constant vertical magnetic field. Here, the novel attitude to single-phase hybrid nanofluid model corresponds to considering nanoparticles and base fluid masses to compute solid equivalent volume fraction, solid equivalent density, and also solid equivalent specific heat at constant pressure. The basic PDEs are transformed into dimensionless ODEs using Von Kármán similarity transformations, which are then solved numerically using bvp4c function. Results indicate that mass suction and magnetic field effects diminish all hydrodynamic and thermal boundary layer thicknesses. Finally, a significant report is presented to investigate quantities of engineering interest due to governing parameters' effects.

Keywords: 3D boundary layer flow; Single-phase hybrid nanofluid; Spinning disk; Semi-analytical modeling; Diathermic oil.

1. Introduction

With the recent improvements in nanotechnology, the production of particles with sizes on the order of nanometers (nanoparticles [1]) can be achieved with relative ease. As a consequence, the idea of suspending these nanoparticles in a base liquid [2] for improving thermal conductivity has been proposed recently. Such suspension of nanoparticles in a base fluid is called a nanofluid [3]. Due to their small size, nanoparticles fluidize easily inside the base fluid, and as a consequence, clogging of channels and erosion in channel walls are no longer a problem. It is even possible to use nanofluids in porous channels [4]. When it comes to the stability of the suspension, it was shown that sedimentation of particles can be prevented by utilizing proper dispersants. Thus, nanofluids are fluids that contain suspensions of nanoparticles of high thermally conductive materials like carbon, metals, and metal oxides into heat transfer fluids to improve the overall thermal conductivity. These nanoparticles are usually of order 100 nm or less. Nanoparticles can be spherical, cylindrical, brick, platelet or blade shapes. The advantages of properly engineered nanofluids according to Ding et al. [5] include these factors: i) higher thermal conductivities than that predicted by currently available macroscopic models, ii) excellent stability, iii) little penalty due to an increase in pressure drop, and iv) little penalty due to an increase in pipe wall abrasion experienced by suspensions of millimeter or micrometer particles [6]. In spite of some inconsistency in the literature and insufficient understanding of the mechanism of the heat transfer in nanofluids, it has emerged as a promising heat transfer fluid. In the continuation of nanofluid research, the researchers have also tried to use hybrid nanofluids, recently, which are engineered by suspending dissimilar nanoparticles either in mixture or composite form. The idea of using hybrid nanofluids is to further improve heat transfer and pressure drop characteristics by a trade-off between advantages and disadvantages of individual suspension attributed to good aspect ratio, better thermal network and synergistic effect of nanomaterials. However, the long-term stability, production

Published online: June 14 2019

process, selection of suitable nanomaterials combination to get synergistic effect and the expense of nanofluids may be major challenges behind the practical applications [7]. The hybrid nanofluids are new types of nanofluids and their performance evaluation is still in the development phase. It is expected to use hybrid nanofluids for similar applications with nanofluid and better performance is expected due to high performance of hybrid nanofluids. A lot of researches related to various applications of nanofluids have been conducted since the discovery of nanofluids. Some of the application areas include electronic cooling, heat pipes, car radiators, coolant in welding and machining, nuclear plant, heat exchanger, solar heating, etc. [8]. Most of the researches about hybrid nanofluids correspond to experimental works [9-14]. Besides, Hayat and Nadeem [15] probably is the first to analytically expand thermophysical properties of hybrid nanofluids in order to develop numerically a boundary layer flow of 3D rotating hybrid nanofluid over a stretching sheet with radiation, heat generation and chemical reaction effects. Furthermore, Chamkha et al. [16] modeled the unsteady conjugate natural convection in a semicircular cavity with a solid shell of finite thickness filled with Al_2O_3-Cu/water hybrid nanofluid by a finite difference method of the second-order accuracy. The obtained results have revealed essential heat transfer enhancement at solid–fluid interface with the addition of nanoparticles. Wei et al. [17] in a pioneering experimental research investigated a kind of hybrid nanoparticles (SiC/TiO_2) with diathermic oil as base fluid to fabricate nanofluids with concentration up to 1 vol% and there was no visually observable sedimentation or stratification even after ten days. The diathermic oil (DO) is a kind of traditional heat transfer fluid commonly used in many fields such as energy storage systems, cooling systems and heating control system [18]. Besides, diathermic oil is very important in those applications where high temperatures are reached or where the use of water or vapor is not suitable. Therefore, an improvement of diathermic oil thermo-physical properties, by using nanoparticles, can increase the performance of the systems [19].

The study of magnetohydrodynamic (MHD) flow has received a great deal of research interest due to its importance in many engineering applications, such as plasma studies, petroleum industries, MHD power generators, cooling of nuclear reactors, the boundary layer control in aerodynamics, and crystal growth [20]. The term "MHD" was first introduced by Alfven [21]. The theory of MHD states that inducing a current in a moving conductive fluid in the presence of magnetic field exerts force on the ions of the conductive fluid [22]. Dinarvand [23] studied the steady 2D flow of an incompressible viscous and electrically conducting fluid over a non-linearly semi-infinite stretching sheet in the presence of a chemical reaction and under the influence of a magnetic field with the help of Homotopy Analysis Method (HAM). Dinarvand et al. [24] also analytically modeled a problem of the steady laminar MHD mixed convection boundary layer flow of a SiO_2-Al_2O_3/water hybrid nanofluid near the stagnation-point on a vertical permeable flat plate with considering dual solutions. Recently, Mehryan et al. [25] worked on the natural convection heat transfer of carbon nanotube-Fe_3O_4/water hybrid nanofluid in a complex porous T-shaped cavity with the heated bottom wall and cold upper one under the effect of inclined uniform magnetic field and local thermal non-equilibrium conditions with inertia terms in the porous model by a finite element method. Moreover, Sheikholeslami et al. [26] attempted to analyze magnetizable hybrid nanofluid of multi-walled carbon nanotube-Fe_3O_4/water inside a circular cavity with two circular heaters. A wire carrying electrical current has been located in the center of each heater. Results show that scattering the hybrid nanoparticles of MWCNT-Fe_3O_4 inside the base fluid increases the convective heat transfer.

The classical Von Kármán [27] problem is the flow close to a flat disk rotating in a fluid which is otherwise at rest with constant angular velocity about an axis perpendicular to its plane. Because of the no-slip condition and the viscosity, the layer of fluid directly at the disk is carried along with it and driven outwards by the centrifugal force. New fluid particles are then continuously pulled onto the disk in the axial direction and then ejected centrifugally again. This is, therefore, a fully three–dimensional flow which acts as a pump [28]. Kármán [27] used this flow to illustrate his celebrated momentum-integral relation derived in the same paper in 1921. In 1934, Cochran [29] improved the accuracy with matched inner and outer expansions. Rogers and Lance [30] in 1960 presented very accurate numerical solutions [31]. The importance of heat transfer from a rotating body can be ascertained in aeronautical science as well as in other engineering branches such as thermal-power generating systems, rotating machinery, medical equipment, computer storage devices, gas turbine rotors, air cleaning machines, electronic devices and crystal growth processes [32]. In 2009, Rashidi and Dinarvand [33] found the totally analytic solutions of the system of nonlinear ordinary differential equations derived from similarity transform for the steady three-dimensional problem of fluid deposition on an inclined rotating disk by using HAM. Moreover, in 2010, Dinarvand [34] also worked on examining the off-centered stagnation flow towards a rotating disc, analytically. Bachok et al. [35] studied the flow and heat transfer characteristics due to a rotating disk immersed in a water-based nanofluid containing different types of nanoparticles: Cu, Al_2O_3 and TiO_2 with exploiting Keller-Box method. The analysis of the second law of thermodynamics applied to an electrically conducting incompressible nanofluid flow with three types of nanoparticles (Cu, CuO and Al_2O_3) over a porous rotating disk in the presence of an externally applied uniform vertical magnetic field with the help of 4^{th} order Runge-Kutta based shooting method investigated by Rashidi et al. [36].

Motivated from above paragraphs, we intend to semi-analytically model the flow and heat transfer of the MHD von Kármán problem with considering a kind of hybrid nanofluid as well as a novel computational procedure that has never utilized before. Our proposed hybrid nanofluid is considered SiC-TiO_2/DO. It is worthwhile to notice that, diathermic oil has high boiling point, low vapor pressure, and low pour point. So, it has been widely used as a heat carrier in heat transfer systems [17]. Moreover, it is assumed that the rotating disk is permeable, the nanoparticles' shape are spherical and the foregoing algorithm proposes the new definition of an equivalent solid volume fraction, solid density and solid specific heat at constant pressure for a hybrid nanofluid that is computed from thermophysical properties of both base fluid and nanoparticles, simultaneously. In all the previous analytical research papers, like Refs. [15, 16, 24-26], the thermophysical properties of the hybrid nanofluid were the functions of volume fraction of first and second nanoparticles. However, in the present paper, we used those properties in terms of masses of both nanoparticles and base fluid. Needless to say, this algorithm is simpler and

better to use relatively. Hence, the exploiting of this algorithm as well as the selection of diathermic oil as the base fluid are novelties of our work. After using similarity transformation method, the nonlinear governing PDEs are altered into the dimensionless nonlinear similarity governing ODEs. Then, the resultant boundary value problem is numerically solved by a famous finite difference scheme named bvp4c built-in function from MATLAB software. Finally, the influence of the governing parameters on the flow and thermal characteristics of the problem is discussed in details.

2. Mathematical Formulation

Let us consider an incompressible viscous laminar and steady SiC-TiO_2/DO hybrid nanofluid flow due to a permeable rotating disk with a constant angular velocity ω which is placed at $z = 0$ in the presence of an externally applied uniform vertical magnetic field B_0 as shown in Fig. 1.

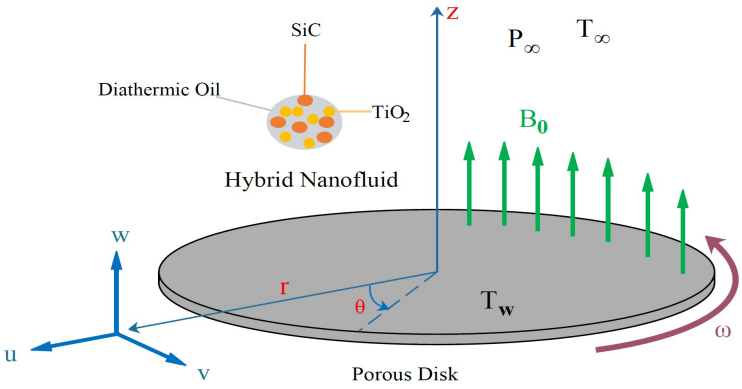

Fig. 1. The schematic diagram of the problem and the coordinate system.

Silicon carbide (SiC) and titanium oxide (TiO_2) are considered as the nanoparticles with diathermic oil (DO) as Newtonian base fluid. The important hypothesis is that the base fluid and nanoparticles are in thermal equilibrium and no slip occurs between them. It is worth mentioning that to analytically develop the targeted hybrid nanofluid (SiC-TiO_2/DO), SiC is initially scattered into base fluid, then, TiO_2 is dispersed in SiC/DO mono-nanofluid. Therefore, the subscript (1) corresponds to the first nanoparticle (SiC), while subscript (2) corresponds to the second nanoparticle (TiO_2) as well as subscript (*f*) is related to the base fluid. Table 1 shows thermophysical properties of diathermic oil, water and the nanoparticles [17, 37-39].

Table 1. Thermophysical properties of the diathermic oil, water and the nanoparticles [17, 37-39].

Thermophysical properties	Water [37]	*DO* [38]	*SiC* [17,39]	TiO_2 [17,39]
C_p (J/kg K)	4179	2030	1340	692
ρ (kg/m^3)	997.1	855	3370	4230
k (W/m K)	0.613	0.133	150	8.4
Particle size (nm)	–	–	30	10

According to Fig. 1, non-rotating cylindrical coordinates system (r, θ, z), is chosen as well as their respective components of velocity (u, v, w). It is assumed that the fluid is infinite and extends in the positive z-direction [35]. The constant temperature of the rotating disk is T_w, while temperature and pressure of the ambient hybrid nanofluid are T_∞ and P_∞, respectively. After using boundary layer approximations as well as the proposed nanofluid's model by Tiwari and Das [40], the dimensional governing non-linear PDEs including conservation of in turn mass, momentum and energy can be written as follows [35,36]:

$$\frac{\partial u}{\partial r}+\frac{u}{r}+\frac{\partial w}{\partial z}=0, \tag{1}$$

$$u\frac{\partial u}{\partial r}+w\frac{\partial u}{\partial z}-\frac{v^2}{r}+\frac{1}{\rho_{hnf}}\frac{\partial P}{\partial r}=\frac{\mu_{hnf}}{\rho_{hnf}}\left(\frac{\partial^2 u}{\partial r^2}+\frac{1}{r}\frac{\partial u}{\partial r}-\frac{u}{r^2}+\frac{\partial^2 u}{\partial z^2}\right)-\frac{\sigma B_0^2}{\rho_{hnf}}u, \tag{2}$$

$$u\frac{\partial v}{\partial r}+w\frac{\partial v}{\partial z}+\frac{uv}{r}=\frac{\mu_{hnf}}{\rho_{hnf}}\left(\frac{\partial^2 v}{\partial r^2}+\frac{1}{r}\frac{\partial v}{\partial r}-\frac{v}{r^2}+\frac{\partial^2 v}{\partial z^2}\right)-\frac{\sigma B_0^2}{\rho_{hnf}}v, \tag{3}$$

$$u\frac{\partial w}{\partial r}+w\frac{\partial w}{\partial z}+\frac{1}{\rho_{hnf}}\frac{\partial P}{\partial z}=\frac{\mu_{hnf}}{\rho_{hnf}}\left(\frac{\partial^2 w}{\partial r^2}+\frac{1}{r}\frac{\partial w}{\partial r}+\frac{\partial^2 w}{\partial z^2}\right), \tag{4}$$

$$u\frac{\partial T}{\partial r}+w\frac{\partial T}{\partial z}=\alpha_{hnf}\left(\frac{\partial^2 T}{\partial r^2}+\frac{1}{r}\frac{\partial T}{\partial r}+\frac{\partial^2 T}{\partial z^2}\right), \tag{5}$$

Subject to these dimensional boundary conditions [35, 36]:

$$\begin{aligned} &u=0, \quad v=\omega\, r, \quad w=w_0, \qquad T=T_w \quad at \quad z=0,\\ &u\to 0, \quad v\to 0, \quad T\to T_\infty, \qquad P\to P_\infty \quad as \quad z\to\infty. \end{aligned} \tag{6}$$

in which T and P are the temperature and the pressure of the hybrid nanofluid within the boundary layer, respectively. σ is the electrical conductivity, w_0 is the uniform suction velocity at the surface of the rotating disk. ρ_{hnf}, $(\rho C_P)_{hnf}$, μ_{hnf}, α_{hnf} and k_{hnf} are the density, the volumetric heat capacity, the viscosity, the thermal diffusivity, and the thermal conductivity of the hybrid nanofluid, respectively. They are defined according to Table 2.

Table 2. Applied models for thermophysical properties of the hybrid nanofluid [15, 24, 41].

Property	Hybrid Nanofluid
Viscosity (μ)	$\dfrac{\mu_f}{(1-\phi)^{2.5}}$
Density (ρ)	$(1-\phi)(\rho_f)+\phi\ (\rho_s)$
Heat capacity (ρC_P)	$\left[(1-\phi)(\rho_f)+\phi(\rho_s)\right]\times\left[(1-\phi)(C_P)_f+\phi(C_P)_s\right]$
Thermal conductivity (k)	$\dfrac{k_2+2k_{nf}-2\phi_2(k_{nf}-k_2)}{k_2+2k_{nf}+\phi_2(k_{nf}-k_2)}\times\dfrac{k_1+2k_f-2\phi_1(k_f-k_1)}{k_1+2k_f+\phi_1(k_f-k_1)}\times(k_f)$
Diffusivity (α)	$\dfrac{k_{hnf}}{(\rho C_p)_{hnf}}$

In Table 2, k_{nf} is the thermal conductivity of the mono-nanofluid which is computed from Maxwell-Garnett model [42]:

$$\frac{k_{nf}}{k_f}=\frac{k_1+2k_f-2\phi_1(k_f-k_1)}{k_1+2k_f+\phi_1(k_f-k_1)}. \tag{7}$$

In this approach, we present ϕ, ρ_s and $(C_P)_s$ as the equivalent nanoparticle's volume fraction, the equivalent density of nanoparticles and the equivalent specific heat at constant pressure of nanoparticles, respectively. ϕ_1 and ϕ_2 as solid fraction of first and second nanoparticles, respectively, which are determined from the following formulas [17, 41, 43]:

$$\rho_s=\frac{(\rho_1\times w_1)+(\rho_2\times w_2)}{w_1+w_2}, \tag{8}$$

$$(C_P)_s=\frac{\{(C_P)_1\times w_1\}+\{(C_P)_2\times w_2\}}{w_1+w_2}, \tag{9}$$

$$\phi_1=\frac{\dfrac{w_1}{\rho_1}}{\dfrac{w_1}{\rho_1}+\dfrac{w_2}{\rho_2}+\dfrac{w_f}{\rho_f}}, \tag{10}$$

$$\phi_2=\frac{\dfrac{w_2}{\rho_2}}{\dfrac{w_1}{\rho_1}+\dfrac{w_2}{\rho_2}+\dfrac{w_f}{\rho_f}}, \tag{11}$$

$$\phi = \phi_1 + \phi_2. \tag{12}$$

In Eqs. (8) to (12), w_1, w_2 and w_f are masses of the first nanoparticle, the second nanoparticle and the base fluid, respectively. By exploiting Von Kármán [27] similarity variables [35, 36]:

$$\begin{aligned} &\eta = \left(\frac{\omega}{\nu_f}\right)^{1/2} z, \qquad u = \omega\, rF(\eta), \qquad v = \omega\, rG(\eta), \\ &w = \left(\omega\nu_f\right)^{1/2} H(\eta), \qquad P - P_\infty = 2\mu_f \omega P(\eta), \qquad \theta(\eta) = \frac{T - T_\infty}{T_w - T_\infty}. \end{aligned} \tag{13}$$

Fortunately, by substituting Eq. (13) into non-linear PDEs (1) to (5) under boundary conditions (6), we get these dimensionless non-linear similarity ODEs:

$$2F + H' = 0, \tag{14}$$

$$A_1 F'' - HF' - F^2 + G^2 - MF = 0, \tag{15}$$

$$A_1 G'' - HG' - 2FG - MG = 0, \tag{16}$$

$$\frac{1}{Pr}\frac{k_{hnf}}{k_f} A_2\, \theta'' - H\theta' = 0, \tag{17}$$

where

$$A_1 = \left(1 - \frac{\frac{w_1}{\rho_1} + \frac{w_2}{\rho_2}}{\frac{w_1}{\rho_1} + \frac{w_2}{\rho_2} + \frac{w_f}{\rho_f}}\right)^{-2.5} \left(1 - \frac{\frac{w_1}{\rho_1} + \frac{w_2}{\rho_2}}{\frac{w_1}{\rho_1} + \frac{w_2}{\rho_2} + \frac{w_f}{\rho_f}} + \frac{\frac{w_1}{\rho_1} + \frac{w_2}{\rho_2}}{\frac{w_1}{\rho_1} + \frac{w_2}{\rho_2} + \frac{w_f}{\rho_f}} \frac{\rho_s}{\rho_f}\right)^{-1}$$

$$A_2 = \frac{(\rho C_P)_f}{\left[\left(1 - \frac{\frac{w_1}{\rho_1} + \frac{w_2}{\rho_2}}{\frac{w_1}{\rho_1} + \frac{w_2}{\rho_2} + \frac{w_f}{\rho_f}}\right)(\rho_f) + \frac{\frac{w_1}{\rho_1} + \frac{w_2}{\rho_2}}{\frac{w_1}{\rho_1} + \frac{w_2}{\rho_2} + \frac{w_f}{\rho_f}}(\rho_s)\right] \times \left[\left(1 - \frac{\frac{w_1}{\rho_1} + \frac{w_2}{\rho_2}}{\frac{w_1}{\rho_1} + \frac{w_2}{\rho_2} + \frac{w_f}{\rho_f}}\right)(C_P)_f + \frac{\frac{w_1}{\rho_1} + \frac{w_2}{\rho_2}}{\frac{w_1}{\rho_1} + \frac{w_2}{\rho_2} + \frac{w_f}{\rho_f}}(C_P)_s\right]} \tag{18}$$

Subject to these dimensionless boundary conditions:

$$\begin{aligned} &F(0) = 0, \qquad G(0) = 1, \qquad H(0) = V_s, \qquad \theta(0) = 1, \\ &F(\infty) \to 0, \qquad G(\infty) \to 0, \qquad \Theta(\infty) \to 0. \end{aligned} \tag{19}$$

We notice that, the parameters that are represented into the boundary value problem (14) to (19) are called “governing parameters”. Here, the governing parameters of the problem are the Prandtl number (Pr), magnetic parameter (M) and suction parameter (V_s) which can be defined as follows:

$$Pr = \frac{\upsilon_f}{\alpha_f}, \qquad M = \frac{\sigma B_0^2}{\rho_{hnf}\omega}, \qquad V_s = \frac{w_0}{\sqrt{\upsilon_f \omega}}, \tag{20}$$

it should be mentioned that other governing parameters of the problem are the nanoparticle masses (w_1, w_2), base fluid mass (w_f), nanoparticles volume fractions (ϕ, ϕ_1, ϕ_2), solid density (ρ_s) and solid specific heat at constant pressure $((C_P)_s)$. The total skin friction coefficient C_f and the local Nusselt number Nu are defined as [36]:

$$C_f = \frac{\sqrt{(\tau_{wr})^2 + (\tau_{w\theta})^2}}{\rho_f (\omega\, r)^2}, \qquad Nu = \frac{rq_w}{k_f (T_w - T_\infty)}, \tag{21}$$

where, τ_{wr} and $\tau_{w\theta}$ are the radial and transversal shear stresses at the surface of the disk, respectively. q_w is the surface heat flux from one, which are illustrated by [36]:

$$\tau_{wr} = \mu_{hnf}\left(\frac{\partial u}{\partial z}+\frac{1}{r}\frac{\partial w}{\partial \theta}\right)_{z=0}, \qquad \tau_{w\theta} = \mu_{hnf}\left(\frac{\partial v}{\partial z}+\frac{1}{r}\frac{\partial w}{\partial \theta}\right)_{z=0}, \qquad q_w = -k_{hnf}\left(\frac{\partial T}{\partial z}\right)_{z=0}, \tag{22}$$

By substituting Eq. (13) into Eqs. (21) and (22):

$$\left[Re\right]^{1/2} C_f = \left(1-\frac{\frac{w_1}{\rho_1}+\frac{w_2}{\rho_2}}{\frac{w_1}{\rho_1}+\frac{w_2}{\rho_2}+\frac{w_f}{\rho_f}}\right)^{-2.5} \sqrt{\{F'(0)\}^2+\{G'(0)\}^2}, \qquad \left[Re\right]^{-1/2} Nu = -\frac{k_{hnf}}{k_f}\theta'(0), \tag{23}$$

where, $Re = \omega r^2/\upsilon_f$ is the local Reynolds number. In summary, it can be depicted that the computational procedure for our proposed algorithm in Fig. 2. According to this figure, initially we must determine our novel inputs such as w_1, w_2 and w_f. In as much as ϕ, ϕ_1, ϕ_2, ρ_s and $(C_P)_s$ are functions of aforementioned masses (see Eqs. (8) to (12)), consequently we can calculate them. Then, we intend to numerically solve the governing Eqs. (14) to (17) along with the boundary conditions (18) and (19), after selecting other governing parameters like M, V_s and Pr. Finally, the results may be plotted through graphical or tabular forms.

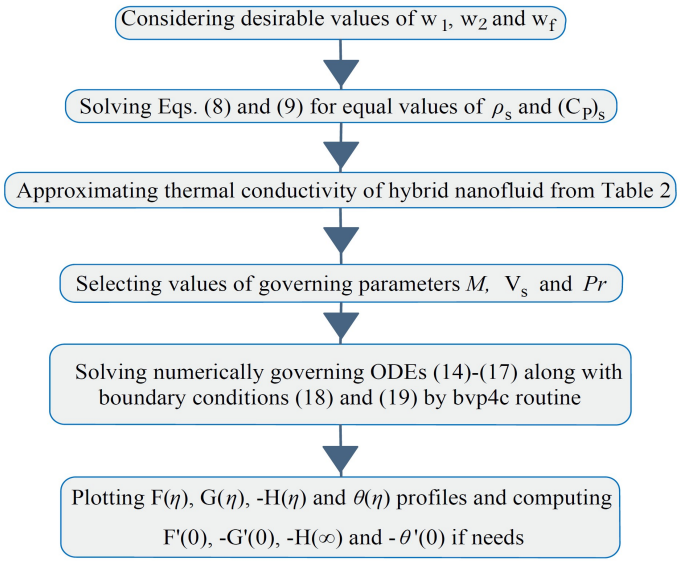

Fig. 2. Flowchart of present problem's computational procedure.

3. Results and Discussion

3.1. Validation of the results

We have to numerically solve the similarity governing Eqs. (14) to (17) subjected to the boundary conditions (18) and (19) for some values of the governing parameters w_1, w_2, w_f, ϕ, ϕ_1, ϕ_2, ρ_s, $(C_P)_s$, M, V_s and Pr using the bvp4c built-in function from MATLAB software (see Shampine et al. [44] as well as Rosca et al. [45]). In this approach, we have considered $5 \le \eta_\infty \le 11$, a uniform initial step size of $\eta_\infty/100$, and the relative tolerance that was set as default (0.001).

As much as there is no numerical work with considering diathermic oil as the working fluid, the numerical procedure must be verified by using water as the base fluid. So, Table 3 shows our validation results from the similarity radial skin friction coefficient $(F'(0))$, the similarity tangential skin friction coefficient $(-G'(0))$, the similarity axial velocity at far field boundary condition $(-H(\infty))$ and the similarity local Nusselt number $(-\theta'(0))$ for pure water $(w_1 = w_2 = \phi = \phi_1 = \phi_2 = 0)$, impermeable rotating disk $(V_s = 0)$, no magnetic field effect $(M = 0)$ and $Pr = 6.2$, respectively. Also, Table 4 illustrates them for a special case (TiO_2/water mono-nanofluid) with various values of w_2 and V_s, when $w_f = 100gr$, $w_1 = \phi_1 = M = 0$ and $Pr = 6.2$. From

Tables 3 and 4, we can clearly conclude that the present results are in good agreement with previous reports obtained by White [31], Schlichting and Gersten [28], Bachok et al. [35], Rashidi et al. [36], Turkyilmazoglu [32] and Yin et al. [46].

Table 3. Validation of the numerical solutions for $F'(0)$, $-G'(0)$, $-H(\infty)$ and $-\theta'(0)$, when $\phi=\phi_1=\phi_2=w_1=w_2=M=V_s=0$, $w_f=100gr$ and $Pr=6.2$.

	White [31]	Schlichting and Gersten [28]	Bachok et al. [35]	Rashidi et al. [36]	Turkyilmazoglu [32]	Yin et al. [46]	Present Study
$F'(0)$	0.51023	0.51023	0.5102	0.510186	0.51023262	0.51022941	0.51021367
$-G'(0)$	0.61592	0.61592	0.6159	0.61589	0.61592201	0.61591990	0.61590956
$-H(\infty)$	0.8838	0.88446	-	-	0.88447411	0.88446912	0.88229879
$-\theta'(0)$	-	-	0.9337	-	0.93387794	0.93387285	0.93384782

Table 4. Validation of the results for $F'(0)$, $-G'(0)$ and $-\theta'(0)$, with different values of w_2 and V_s when $w_f=100gr$, $w_1=\phi_1=M=0$ and $Pr=6.2$.

$w_2(gr)$	$\phi=\phi_2$	V_s	$F'(0)$		$-G'(0)$		$-\theta'(0)$		
			Bachok et al. [35]	Present study	Bachok et al. [35]	Present study	Bachok et al. [35]	Turkyilmazoglu [32]	Present study
50	0.10	0	0.5102	0.514633	0.6159	0.621243	0.8344	0.83557817	0.83081098
50	0.10	-1	0.3896	0.387604	1.1752	1.194499	4.8254	-	4.763264
50	0.10	1	0.4896	0.492917	0.3022	0.302486	0.0013	-	0.001359
23	0.05	0	-	-	-	-	-	0.88399909	0.88264795
76	0.15	0	-	-	-	-	-	0.78891926	0.78642403
107	0.20	0	-	-	-	-	-	0.74412223	0.74208425

3.2. Effects of the governing parameters on the dimensionless velocity and temperature profiles

Hereafter, the effect of aforementioned governing parameters on the flow and heat transfer characteristics of the problem, are portrayed as graphical figures. At first, it is useful to determine ranges of governing parameters in the present study as shown in Table 5.

Table 5. The applied range of governing parameters in the present analysis.

Governing parameter	Symbol	Value
Mass of the first nanoparticle	w_1	{0,10}
Mass of the second nanoparticle	w_2	{0,10,15,23,30,50,76,107}
Mass of the base fluid	w_f	{100}
Magnetic parameter	M	{0,1,2,3}
Suction parameter	V_s	{-1,-0.5,0,1}
Prandtl number	Pr	{6.2,395}

Figures 3 to 6 illustrate the effect of the magnetic parameter (M), the suction parameter (V_s) and the second nanoparticle's mass (w_2) with considering $w_f=100gr$, $w_1=10gr$ and $Pr=395$, on the dimensionless fluid velocity components in radial, tangential and axial directions as well as on the dimensionless temperature distribution, respectively. From Figs. 3 and 4, it can be seen that $F(\eta)$, $G(\eta)$ as well as radial and tangential dimensionless hydrodynamic boundary layer thicknesses decrease, under the same three foregoing parameters effects. Moreover, with increasing M the Lorentz force effects lead to enhancement and it affects both radial and tangential dimensionless velocity profiles. It is worth noticing that when the suction parameter enhances, the radial and tangential dimensionless hydrodynamic boundary layer thicknesses decrease, too. On the other hand, among these three governing parameters, M has the maximum influence on $F(\eta)$ as well as $G(\eta)$. This is because the magnetic parameter appears directly into the similarity momentum equation along with radial and tangential directions (equations (15) and (16)).

Figure 5 (axial component of dimensionless velocity profiles) acts differently relative to Figs. 3 and 4 (radial and tangential components of dimensionless velocity field). In other words, although increasing suction parameter decreases the axial dimensionless velocity profiles, enhancing of magnetic parameter as well as second nanoparticle's mass help to elevate $H(\eta)$. It is also shown that the mass suction decline at the surface of the rotating disk possesses maximum effects on $H(\eta)$ profiles.

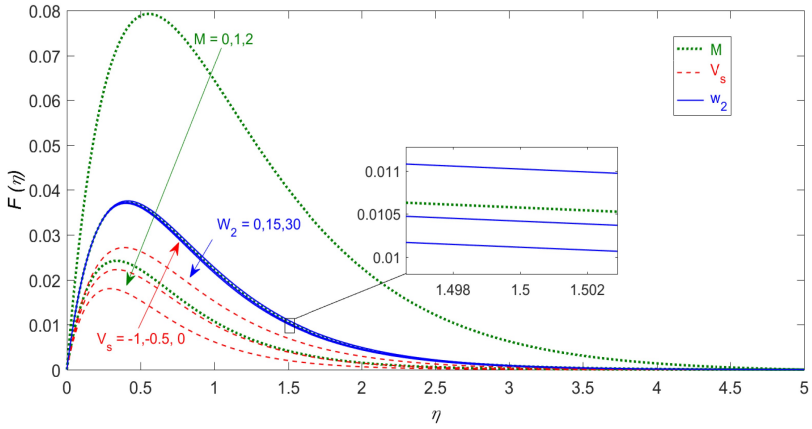

Fig. 3. Effect of magnetic parameter (M), suction parameter (V_s) and second nanoparticle's mass (w_2) on the dimensionless velocity profiles along the radial direction ($F(\eta)$), when $w_f = 100gr$, $w_1 = 10gr$ and $Pr = 395$.

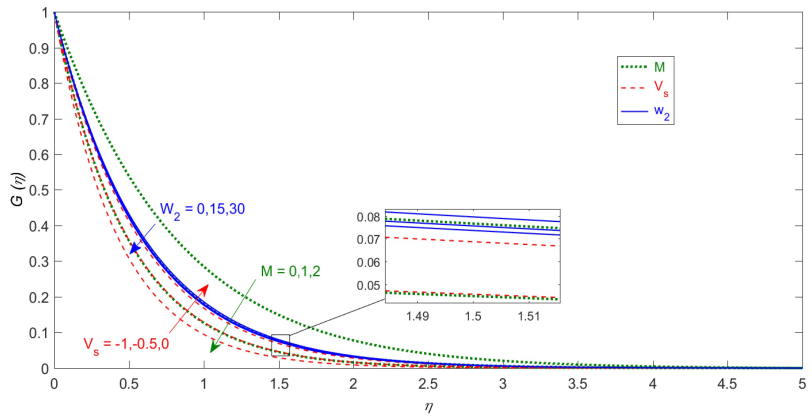

Fig. 4. Effect of magnetic parameter (M), suction parameter (V_s) and second nanoparticle's mass (w_2) on the dimensionless velocity profiles along the tangential direction ($G(\eta)$), when $w_f = 100gr$, $w_1 = 10gr$ and $Pr = 395$.

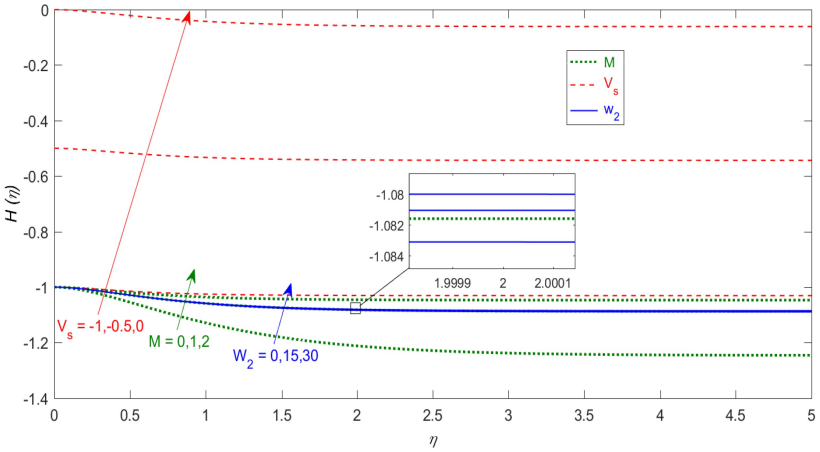

Fig. 5. Effect of magnetic parameter (M), suction parameter (V_s) and the second nanoparticle's mass (w_2) on the dimensionless velocity profiles along axial direction ($H(\eta)$), when $w_f = 100gr$, $w_1 = 10gr$ and $Pr = 395$.

As a result of Fig. 6, the influence of w_2 and M on the dimensionless temperature field can be considered negligible, while the effect of V_s on it, is strongly high. Indeed, the thermal boundary layer thickness, as well as the dimensionless temperature distribution decreases with increasing in suction parameter. This behavior as will be seen subsequently leads to local heat transfer rate enhancement from the rotating disk to ambient (see Fig. 8 (b)).

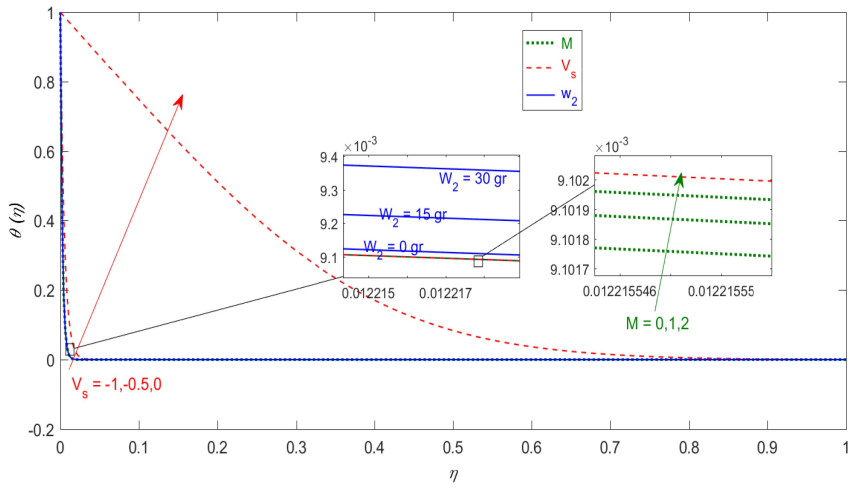

Fig. 6. Effect of magnetic parameter (M), suction parameter (V_s) and second nanoparticle's mass (w_2) on the dimensionless temperature distributions ($\theta(\eta)$), when $w_f = 100gr$, $w_1 = 10gr$ and $Pr = 395$.

3.3. Effects of governing parameters on skin friction and local heat transfer rate

Figures 7 (a) and (b) are plotted to compare in turn the total skin friction coefficient ($[Re]^{1/2} C_f$) and the local heat transfer rate ($[Re]^{-1/2} Nu$) for various values of second nanoparticle's mass (w_2), when $w_f = 100gr$, $w_1 = 10gr$, $M = 1$, $V_s = -1$ and $Pr = 395$. As can be seen, both $[Re]^{1/2} C_f$ and $[Re]^{-1/2} Nu$ slowly boost under enhancing of w_2, that can be sensible physically. When w_2 increases, the second nanoparticle's volume fraction (ϕ_2) as well as the solid equivalent volume fraction (ϕ) increase, consequently, the effective thermal conductivity (k_{hnf}) enhances. So, according to Eq. (23) the local heat transfer rate elevates.

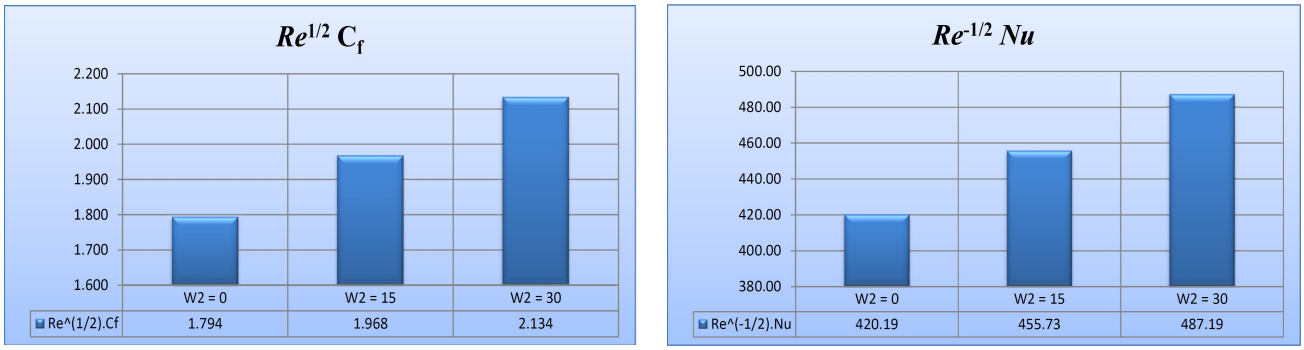

(a) (b)

Fig. 7. Effect of second nanoparticle's mass (w_2) on (a) the total skin friction coefficient ($[Re]^{1/2} C_f$) and (b) the local heat transfer rate ($[Re]^{-1/2} Nu$) of the rotating disk, when $w_f = 100gr$, $w_1 = 10gr$, $M = 1$, $V_s = -1$ and $Pr = 395$.

Figures 8 (a) and (b) depict $[Re]^{1/2} C_f$ and $[Re]^{-1/2} Nu$ for various values of the suction parameter (V_s), when $w_f = 100gr$, $w_1 = w_2 = 10gr$, $M = 3$ and $Pr = 395$. It is obvious that, suction parameter affects the total skin friction coefficient as well as the local heat transfer rate enhancement, simultaneously. It should be highlighted that according to Eq. (23), another important factors that influences $[Re]^{1/2} C_f$ and $[Re]^{-1/2} Nu$ enhancement depends on the dimensionless velocity profiles slope at $\eta = 0$ along the radial and tangential directions ($F'(0)$ and $G'(0)$) as well as the dimensionless temperature profile's slope at one ($\theta'(0)$). As a consequence, inasmuch as from Figs. 3, 4 and 6, the foregoing slopes generally increase, so we observed increment in $[Re]^{1/2} C_f$ and $[Re]^{-1/2} Nu$.

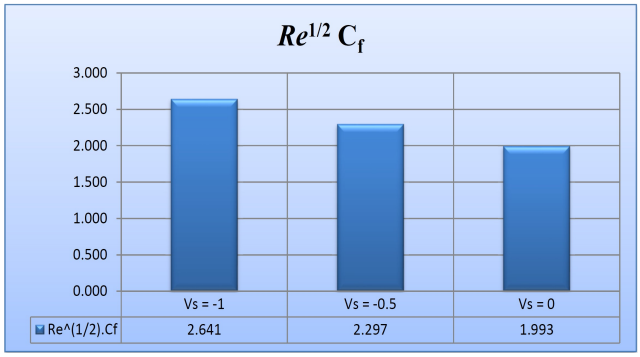

(a)

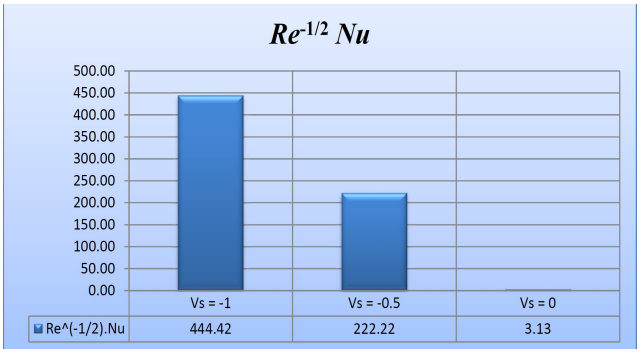

(b)

Fig. 8. Effect of the suction parameter (V_s) on (a) the total skin friction coefficient ($[Re]^{1/2} C_f$) and (b) the local heat transfer rate ($[Re]^{-1/2} Nu$) of the rotating disk, when $w_f = 100gr$, $w_1 = w_2 = 10gr$, $M = 3$ and $Pr = 395$.

Finally, Figs. 9 (a) and (b) demonstrate $[Re]^{1/2} C_f$ and $[Re]^{-1/2} Nu$ for various values of magnetic parameter (M), when $w_f = 100gr$, $w_1 = w_2 = 10gr$, $V_s = -1$ and $Pr = 395$. According to our conclusions from previous figures, we can declare that M highly affects the flow field characteristics and its variations on the thermal characteristics is negligible because M does not appear in the similarity energy Eq. (17). Therefore, $[Re]^{1/2} C_f$ only increases with magnetic field effect in the present conditions of the problem.

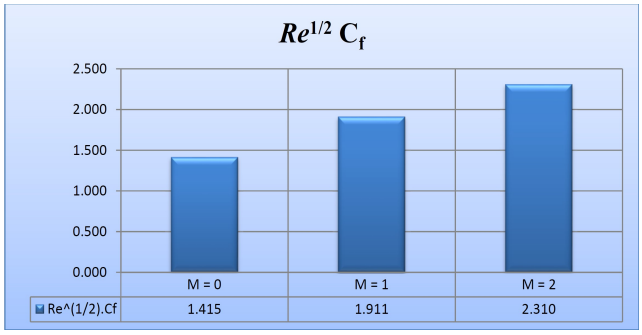

(a)

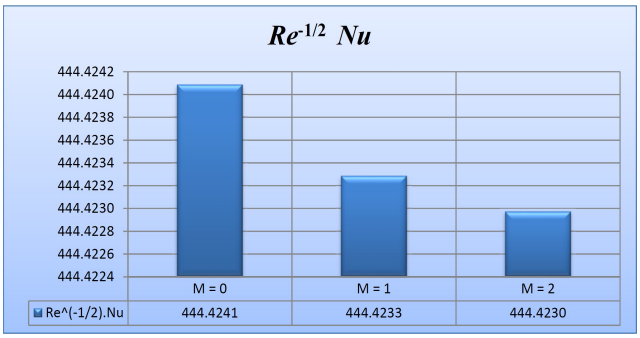

(b)

Fig. 9. Effect of magnetic field (M) on (a) the total skin friction coefficient ($[Re]^{1/2} C_f$) and (b) the local heat transfer rate ($[Re]^{-1/2} Nu$) of the rotating disk, when $w_f = 100gr$, $w_1 = w_2 = 10gr$, $V_s = -1$ and $Pr = 395$.

4. Conclusions

The steady laminar 3D forced convective Von Kármán problem with considering permeable spinning disk and incompressible SiC-TiO_2-DO hybrid nanofluid as the working fluid in the presence of uniform magnetic field along with vertical direction is investigated semi-analytically by a new proposed algorithm according to nanoparticle and base fluid masses. It is worth noticing that this research may be applicable in rotating MHD energy generators for new space systems and thermal conversion mechanisms for nuclear propulsion space vehicles. The Prandtl number of the base fluid (diathermic oil) is kept constant at 395 and the nanoparticles are assumed to be spherical shapes. After using boundary layer approximations as well as Tiwari-Das nanofluid model, the non-linear governing PDEs are first transformed into non-linear dimensionless ODEs using Von Kármán proposed similarity variables, before being solved numerically by a ready finite difference scheme from MATLAB software. The major conclusions of this study can be summarized as follows:

1) Mass suction and magnetic field effects reduce both radial and tangential hydrodynamic boundary layer thicknesses as well as thermal boundary layer thickness.

2) Increasing w_2 and V_s cause local heat transfer rate enhancement from the rotating disk surface to the ambient and drag force increment from the ambient to the rotating disk, simultaneously; so the local heat transfer rate enhancement has a desirable effect while the skin friction coefficient increment possesses an undesirable effect because of increasing pressure drop and consequently increasing pumping power that always is managed.

3) The present computational algorithm successfully works for hybrid nanofluid problems with great confidence to study the flow and heat transfer characteristics in the other similar geometries.

Acknowledgments

The authors wish to thank the editor and reviewers for their careful, unbiased and constructive suggestions, which led to this revised manuscript.

Conflict of Interest

The authors declared no potential conflicts of interest with respect to the research, authorship and publication of this article.

Funding

The authors received no financial support for the research, authorship and publication of this article.

Nomenclature

B_0	Uniform magnetic field [T]
C_f	Total skin friction coefficient
C_P	Specific heat at constant pressure [J/(kg.K)]
k	Thermal conductivity coefficient [W/(m.K)]
M	Magnetic parameter
Nu	Local Nusselt number
P	Hybrid nanofluid pressure [Pa]
P_∞	Ambient hybrid nanofluid pressure [Pa]
Pr	Prandtl number
q_w	Surface heat flux [W/m^2]
r, θ, z	Cylindrical coordinates system
Re	Local Reynolds number
T	Hybrid nanofluid temperature [K]
T_w	Disk temperature [K]
T_∞	Ambient temperature [K]
u, v	Velocity components along r and θ axes [m/s]
V_s	Suction parameter
w	Mass or velocity component along z axis [gr or m/s]
w_0	Uniform suction velocity at the disk surface [m/s]

Greek symbols

α	Thermal diffusivity [m^2/s]
ϕ	Equivalent nanoparticle volume fraction
ϕ_1	First nanoparticle's volume fraction
ϕ_2	Second nanoparticle's volume fraction
η	Independent similarity variable
$F(\eta)$	Dimensionless radial velocity profile
$G(\eta)$	Dimensionless tangential velocity profile
$H(\eta)$	Dimensionless axial velocity profile
$\theta(\eta)$	Dimensionless temperature profile
σ	Electrical conductivity [(m^{3}A^2)/kg]
μ	Dynamic viscosity [Pa.s]
υ	Kinematic viscosity [m^2/s]
ω	Constant angular velocity [rad/s]
ρ	Density [kg/m^3]
ρC_P	Volumetric heat capacity [J/(m^3 K)]
τ_{wr}	Radial shear stress at the surface of the disk [Pa]
$\tau_{w\theta}$	Transversal shear stress at the surface of the disk [Pa]

Subscripts

s	Solid phase
w	Condition at the surface of the disk
∞	Condition at the ambient
f	Base fluid
nf	Single nanoparticle nanofluid
hnf	Hybrid nanofluid
1	First nanoparticle (SiC)
2	Second nanoparticle (TiO_2)

Superscript

prime	Differentiation with respect to η

References

[1] Sobamowo, M.G., Free convection flow and heat transfer of nanofluids of different shapes of nano-sized particles over a vertical plate at low and high Prandtl numbers, *Journal of Applied and Computational Mechanics*, 5(1), 2019, 13–39.
[2] Kezzar, M., Rafik Sari, M., Bourenane, R., Rashidi, M.M., Haiahem, A., Heat transfer in hydro-magnetic nano-fluid flow between non-parallel plates using DTM, *Journal of Applied and Computational Mechanics*, 4(4), 2018, 352–364.
[3] Ghahremani E., Ghaffari, R., Ghadjari, H., Mokhtari, J., Effect of variable thermal expansion coefficient and nanofluid properties on steady natural convection in an enclosure, *Journal of Applied and Computational Mechanics*, 3(4), 2017, 240–250.
[4] Akinshilo, A.T., Sobamowo, G.M., Perturbation solutions for the study of MHD blood as a third grade nanofluid transporting gold nanoparticles through a porous channel, *Journal of Applied and Computational Mechanics*, 3(2), 2017, 103–117.
[5] Ding, Y., Alias, H., Wen, D., Williams, R.A., Heat transfer of aqueous suspensions of carbon nanotubes (CNT nanofluids), *International Journal of Heat and Mass Transfer*, 49, 2006, 240–250.
[6] Minea, A.A., *Advances in Industrial Heat Transfer*, CRC Press, 2013.

[7] Minea, A.A., A review on the thermophysical properties of water-based nanofluids and their hybrids, *The Annals of "DUNAREA DE JOS" University of GALATI*, 083X, 2016, 35-47.
[8] Sidik, C., Azwadi, N., Adamu, I.M., Jamil, M.M., Kefayati, G.H.R., Mamat, R., Najafi, G., Recent progress on hybrid nanofluids in heat transfer applications: A comprehensive review, *International Communications in Heat and Mass Transfer*, 78, 2016, 68–79.
[9] Madhesh, D., Parameshwaran, R., Kalaiselvam, S., Experimental investigation on convective heat transfer and rheological characteristics of Cu-TiO_2 hybrid nanofluids, *Experimental Thermal and Fluid Science*, 52, 2014, 104–115.
[10] Senthilaraja, S., Vijayakumar, K., Ganadevi, R., A comparative study on thermal conductivity of Al_2O_3/water, CuO/water and Al_2O_3– CuO/water nanofluids, *Digest Journal of Nanomaterials and Biostructures*, 10, 2015, 1449–1458.
[11] Bhosale, G.H., Borse, S.L., Pool Boiling CHF Enhancement with Al_2O_3-CuO/H_2O Hybrid Nanofluid, *International Journal of Engineering Research & Technology*, 2(10), 2013, 946–950.
[12] He, Y., Vasiraju, S., Que L., Hybrid nanomaterial-based nanofluids for micropower generation, *RSC Advances*, 4, 2014, 2433-2439.
[13] Esfe, M.H., Abbasian Arani, A.A., Rezaie, M., Yan, Wei-Mon, Karimipour, A., Experimental determination of thermal conductivity and dynamic viscosity of Ag–MgO/water hybrid nanofluid, *International Communications in Heat and Mass Transfer*, 66, 2015, 189–195.
[14] Syam Sundar, L., Irurueta G.O., Venkata Ramana E., Singh, M,K., Sousa, A.C.M., Thermal conductivity and viscosity of hybrid nanofluids prepared with magnetic nanodiamond-cobalt oxide (ND-Co_3O_4) nanocomposite, *Case Studies in Thermal Engineering*, 7, 2016, 66–77.
[15] Hayat, T., Nadeem, S., Heat transfer enhancement with Ag–CuO/water hybrid nanofluid, *Results in Physics*, 7, 2017, 2317–2324.
[16] Chamkha, A.J., Miroshnichenko, I.V., Sheremet, M.A., Numerical analysis of unsteady conjugate natural convection of hybrid water-based nanofluid in a semicircular cavity, *Journal of Thermal Science and Engineering Applications*, 9, 2017, 041004–9.
[17] Wei, B., Zou, C., Yuan, X., Li, X., Thermo-physical property evaluation of diathermic oil based hybrid nanofluids for heat transfer applications, *International Journal of Heat and Mass Transfer*, 107, 2017, 281–287.
[18] Li, X., Zou, C., Zhou, L., Qi, A., Experimental study on the thermo-physical properties of diathermic oil based SiC nanofluids for high temperature applications, *International Journal of Heat and Mass Transfer*, 97, 2016, 631–637.
[19] Colangelo, G., Favale, E., de Risi, A., Laforgia, D., Results of experimental investigations on the heat conductivity of nanofluids based on diathermic oil for high temperature applications, *Applied Energy*, 97, 2012, 828–833.
[20] Tamim, H., Dinarvand, S., Hosseini, R., Pop, I., MHD mixed convection stagnation-point flow of a nanofluid over a vertical permeable surface: a comprehensive report of dual solutions, *Heat and Mass Transfer*, 50, 2014, 639–650.
[21] Alfven, H., Existence of electromagnetic-hydrodynamic waves, *Nature,* 150, 1942, 405-406.
[22] Domairry Ganji, D., Hashemi Kachapi, S.H., *Application of Nonlinear Systems in Nanomechanics and Nanofluids (Analytical Methods and Applications)*, Elsevier, 2015.
[23] Dinarvand, S., A reliable treatment of the homotopy analysis method for viscous flow over a non-linearly stretching sheet in presence of a chemical reaction and under influence of a magnetic field, *Central European Journal of Physics*, 7(1), 2009, 114-122.
[24] Nademi Rostami, M., Dinarvand, S., Pop, I., Dual solutions for mixed convective stagnation-point flow of an aqueous silica –alumina hybrid nanofluid, *Chinese Journal of Physics*, 56, 2018, 2465-2478.
[25] Mehryan, S.A.M., Sheremet, M.A., Soltani, M., Izadi, M., Natural convection of magnetic hybrid nanofluid inside a double-porous medium using two-equation energy model, *Journal of Molecular Liquids,* 277, 2019, 959–970.
[26] Sheikholeslami, M., Mehryan, S.A.M., Shafee, A., Sheremet, M.A., Variable magnetic forces impact on magnetizable hybrid nanofluid heat transfer through a circular cavity, *Journal of Molecular Liquids*, 277, 2019, 388–396.
[27] Von Kármán, T., Über laminare und turbulente Reibung, *Zeitchrift für Angewandte Mathematik und Mechanik*, 1(4), 1921, 233–252.
[28] Schlichting, H., Gersten, K., *Boundary-Layer Theory*, 9th ed., Springer, 2017.
[29] Cochran, W.G., The flow due to a rotating disk, *Cambridge Philosophical Society*, 30(3), 1934, 365-375.
[30] Rogers, M.G., Lance, G.N., The Rotationally Symmetric Flow of a Viscous Fluid in the Presence of an Infinite Rotating Disk, *Journal of Fluid Mechanics,* 7, 1960, 617-631.
[31] White, F.M., *Viscous Fluid Flow*, 3rd ed., McGraw-Hill, 2006.
[32] Turkyilmazoglu, M., Nanofluid flow and heat transfer due to a rotating disk, *Computers & Fluids*, 94, 2014, 139–146.
[33] Rashidi, M.M., Dinarvand, S., Purely analytic approximate solutions for steady three-dimensional problem of condensation film on inclined rotating disk by homotopy analysis method, *Nonlinear Analysis: Real World Applications*, 10, 2009, 2346–2356.
[34] Dinarvand, S., On explicit, purely analytic solutions of off-centered stagnation flow towards a rotating disc by means of HAM, *Nonlinear Analysis: Real World Applications*, 11, 2010, 3389-3398.
[35] Bachok, N., Ishak, A., Pop, I., Flow and heat transfer over a rotating porous disk in a nanofluid, *Physica B*, 406, 2011, 1767–1772.
[36] Rashidi, M.M., Abelman, S., Freidooni Mehr, N., Entropy generation in steady MHD flow due to a rotating porous disk in ananofluid, *International Journal of Heat and Mass Transfer*, 62, 2013, 515–525.

[37] Dinarvand, S., Pop, I., Free-convective flow of copper/water nanofluid about a rotating down-pointing cone using Tiwari-Das nanofluid scheme, *Advanced Powder Technology*, 28, 2017, 900–909.
[38] Hekmatipour, F., Akhavan-Behabadi, M.A., Sajadi, B., Combined free and forced convection heat transfer of the copper oxide-heat transfer oil (CuO-HTO) nanofluid inside horizontal tubes under constant wall temperature, *Applied Thermal Engineering*, 100, 2016, 621–627.
[39] Kamyar, A., Saidur, R., Hasanuzzaman, M., Application of Computational Fluid Dynamics (CFD) for nanofluids, *International Journal of Heat and Mass Transfer*, 55, 2012, 4104–4115.
[40] Tiwari, R.J., Das, M.K., Heat transfer augmentation in a two sided lid-driven differentially heated square cavity utilizing nanofluids. *International Journal of Heat and Mass Transfer*, 50, 2007, 2002–2018.
[41] Syam Sundar, L., Sharma, K.V., Singh, M.K., Sousa, A.C.M., Hybrid nanofluids preparation, thermal properties, heat transfer and friction factor – A review, *Renewable and Sustainable Energy Reviews*, 68, 2017, 185–198.
[42] Oztop, H.F., Abu-Nada, E., Numerical study of natural convection in partially heated rectangular enclosures filled with nanofluids, *International Journal of Heat and Fluid Flow*, 29, 2008, 1326–1336.
[43] Syam Sundar, L., Venkata Ramana, E., Graça, M.P.F., Singh, M.K., Sousa, A.C.M., Nanodiamond-Fe_3O_4 nanofluids: Preparation and measurement of viscosity, electrical and thermal conductivities, *International Communications in Heat and Mass Transfer*, 73, 2016, 62–74.
[44] Shampine, L.F., Gladwell, I., Thompson, S., *Solving ODEs with MATLAB*, Cambridge University Press, 2003.
[45] Roşca, N.C., Roşca, A.V., Aly, E.H., Pop, I., Semi-analytical solution for the flow of a nanofluid over a permeable stretching/shrinking sheet with velocity slip using Buongiorno mathematical model, *European Journal of Mechanics B/Fluids*, 58, 2016, 39–49.
[46] Yin, C., Zheng, L., Zhang, C., Zhang, X., Flow and heat transfer of nanofluids over a rotating disk with uniform stretching rate in the radial direction, *Propulsion and Power Research*, 6(1), 2017, 25–30.